Science and Technology of Advanced Materials

ISSN: 1468-6996 (Print) 1878-5514 (Online) Journal homepage: www.tandfonline.com/journals/tsta20

Design of open systems for meniscus splitting demonstrated using an aqueous polymer solution

Reina Hagiwara & Kosuke Okeyoshi

To cite this article: Reina Hagiwara & Kosuke Okeyoshi (28 May 2025): Design of open systems for meniscus splitting demonstrated using an aqueous polymer solution, Science and Technology of Advanced Materials, DOI: 10.1080/14686996.2025.2512704

To link to this article: https://doi.org/10.1080/14686996.2025.2512704

Publisher: Taylor & Francis & The Author(s). Published by National Institute for Materials Science in partnership with Taylor & Francis Group.

Journal: Science and Technology of Advanced Materials

DOI: 10.1080/14686996.2025.2512704

Design of open systems for meniscus splitting demonstrated using an aqueous polymer solution

Reina Hagiwara[1], Kosuke Okeyoshi[1*]

[1]*Graduate School of Advanced Science and Technology, Japan Advanced Institute of Science and Technology, 1-1 Asahidai, Nomi, Ishikawa 923-1292, Japan*

*To whom correspondence should be addressed:

E-mail: okeyoshi@jaist.ac.jp

Design of open systems for meniscus splitting demonstrated using an aqueous polymer solution

Open systems on the surfaces of soft materials induce dissipative structures such as evaporative self-organization. Based on the viscous fingering phenomena, we demonstrate a meniscus splitting phenomena by evaporating an aqueous solution of versatile polyvinyl alcohol (PVA) solution from a Hele–Shaw cell. To understand it as a universal phenomenon independent of the polymer species, the distinct evolutionary pathways to pattern formation were evaluated, focusing on the interface deformation and directional deposition of the polymer. The PVA solution, which showed a steep concentration-dependent viscosity gradient under a local moderate humidity gradient, was capable of bridging the cell gap for vertical membrane formation. The interfacial shape transformation from one downward concave to multiple upward convex shapes is controllable not only by tuning the physical properties of the polymer but also by conditioning the water evaporating atmosphere. We envision that demonstrations with different cell aperture designs will expand the realization of this phenomenon using other synthetic polymers or chemical species. Such an open system design with humidity tuning is a strategy for exposure to non-equilibrium phenomena using various soft materials, particles, fibers, and networks.

Keywords: humidity, evaporation rate, polyvinyl alcohol, meniscus splitting, dissipative structure

Introduction

One of the dissipative structures [1], viscous fingering [2–4], is a well-known phenomenon showing that interfacial instability [5] on the surfaces of soft materials and geometrical deformation. When soft materials are in a fluid state in a drying environment, various physicochemical processes [6–8] such as flow [9–14], diffusion [15–17], phase separation [18,19], and gelation [20–23] occur in a non-equilibrium state. This mass influx/efflux contributes to the organized structure of the dried state, such as crystal growth. As one of the pattern formations resulting from the drying of viscous polymer solutions, we recently reported a "meniscus splitting phenomenon" [24-27]. This characteristic time evolution of splitting one meniscus into multiple with spontaneous spatial patterns under non-equilibrium interfacial conditions during solvent evaporation, like drying-induced pattern formation [28-30]. This is an expansion of viscous fingering, changing the interface from an even shape to a wave shape [31-33]. When the solvent of the polymer solution evaporates in a cell with a gap of ~1 mm, the capillary forces acting on the evaporative interface cause the polymer to deposit by bridging the cell gap at multiple specific positions within the characteristic interval. Previously, the meniscus splitting phenomenon has been demonstrated with high reproducibility using several natural polysaccharides such as pectin [34,35] and chitosan [36]. Because polysaccharides exist in harmony with water in vivo, their drying and wetting interface is highly functional as they not only act as nutrient storage mediators in aqueous environments but also as moisturizers in dry-air environments.

However, the interfacial deformation processes immediately before meniscus splitting are assumed to follow solvent evaporation, and it is essential to prove the universality of this phenomenon by demonstrating its species independence. As the first step, we choose polyvinyl alcohol (PVA), a versatile synthetic polymer possessing biocompatible and biodegradable properties and has a high affinity for water. PVA is a representative

hydrophilic synthetic polymer with a chemical structure containing many hydroxy groups. The strategy is to extend the chemical species having similar properties originating from functional groups, as previously demonstrated in polysaccharides. PVA has a simple polymeric structure and a different backbone to polysaccharides such as pectin.

In this study, we designed an open system for the meniscus splitting of an aqueous PVA solution by controlling the vapor phase space for the influx/efflux speed of air containing water vapor. This space control caused substantial local humidity just above the evaporative interface. An aqueous PVA solution was used as the liquid phase to demonstrate its versatility and universality in open systems. As shown in **Fig. 1**, two types of interfacial deformation and characteristic polymer deposition can be controlled by adjusting the humidity through changing the aperture design. Different from polysaccharides forming vertical membranes by splitting the evaporative interface [27], PVA deposition occurs along the horizontal direction when the top of the cell is fully open. This would be because the dehydration of PVA happens much more immediately and bridges the gap on a wide area of the evaporative interface. The rapid evaporation of water from the interface in contact with dry air causes downward convex interface deformation near the center of the cell. As horizontal film formation maintains high humidity, polymer deposition contributes to membrane growth in the vertical direction. In contrast, a partially open aperture suppresses water evaporation and maintains high humidity during the initial drying process. This condition induces the evaporative interface to deform with an upward convexity, and polymer deposition results in vertical membrane formation, similarly seen in polysaccharide solutions in previous works. To test this hypothesis, we investigated the fluid system by focusing on the fundamental properties of the polymer solution, such as its viscosity and the size and position of the apertures.

Results and Discussion

Two different molecular weight PVA (18 and 166 kg/mol) aqueous solutions were dried from a limited space under constant temperature and controlled relative humidity (60 °C and ~5% RH), based on previous studies (**Supporting Information, Fig. S1**) [24]. **Fig. 2A** and **Supporting Information, Movie S1** show the drying process depending on the molecular weight and initial concentration. For the low molecular weight and low initial concentration case (18k-10 wt%), there was no change in the shape of the interface until just before the end of drying. After a monotonous descent, the interface moved horizontally, forming a horizontal film parallel to the *X* direction on the bottom of the cell. In contrast, at a higher initial concentration (18k-30 wt%), the interfacial behavior in the early drying stage became complex. Hole-like sinking of the interface occurred at the beginning of the drying process. This air hole extended in the *X* direction while maintaining its curvature. This is due to the capillary forces, which is strongly affected by the surface tension. When it contacted the sidewall, it sank slightly in the *Z* direction and extended in the opposite *X* direction. The sinking and horizontal deformation of the interface were repeated, resulting in the formation of several horizontal films.

The air holes formed in the initial phase were reproducible regardless of the cell *X*-width. The formation of air holes and their subsequent horizontal deformation can be attributed to the interplay of capillary forces, solvent evaporation rates, and the inherent properties of the PVA solution. **Fig. 2B** shows the results of the geometric analysis of the air holes. The interface shape of the hole-like sinks observed 1 h after the start of drying for the 18k-30 wt% sample was measured. The area of the circular sink is determined by approximating a regular circle, X_c is the distance from the sidewall to the center of the circle, and ΔX is the width of the interface where the sinking occurred. These values were plotted against the *X*-width of the cell. The area of the air holes varied regardless of the *X*-width;

however, the maximum value increased proportionally. The X_c values, which indicate the location of the holes, are distributed between half and quarter of the cell width, indicated by the auxiliary lines in the graph. Furthermore, ΔX increased in proportion to the increase in X-width, consistently equating approximately one-fifth of the X-width. From these geometric analyses, the formation of air holes was observed for all cell sizes, but the hole location and width depended on the X-width of the cell, which suggests that the convection of air in the limited space is a determining factor. Although the width of the sink is affected by the cell width, the area of the hole is independent, indicating that the circular sink region remains fluid and does not dry. Owing to the instability of this region, it is assumed to be a limit on its size and ability to expand horizontally along the top of the solidified horizontal films.

In the higher molecular weight 166k-10 wt% PVA case, stepwise horizontal films and a short vertical membrane were formed (see **Fig. 2A**). Interfacial behavior similar to that of the 18k-30 wt% PVA solution was also observed. After the horizontal deformation of the interface, it became a meniscus, resembling the initial state, and formed a vertical membrane. The solidification process of the horizontal film and the formation of the nucleus as the origin of the vertical membrane were considered to proceed as shown in **Fig. 2C**. Initially, the entire area at the evaporation interface remained fluid, and the contact area with the sidewall was pinned. The solute concentration near the sidewall increased because of capillary flow, leading to solidification on the surface in contact with dry air. The effect of capillary flow was observed from the sidewall to a quarter of the cell width, and the solidified area extended to the inside of the cell. The interface that maintained fluidity near the center of the cell width was deformed to reduce the volume of the liquid phase. At this point, the sinking of the interface was observed as the formation of a new concave meniscus with a different curvature. This depression was uniform until it was pressurized to the point where the Laplace pressure became zero, when it deformed into a circular shape. However, uneven

atmospheric pressure is caused by convection of the gas phase and differences in humidity owing to differences in evaporation rates, with the solidification area acting as a barrier, thus causing the interface to expand horizontally. When a stepwise horizontal film is formed by the deformation front propagating horizontally, it behaves as a lid to maintain a high humidity at the interface, thus inhibiting solidification. In this state, nucleation occurs via self-organization through polymer entanglement.

The measurement of physical parameters revealed a difference in the interface shape transition, which depended on the initial concentration of the aqueous solution and the molecular weight of PVA. The properties of PVA depend on the molecular weight, which indicates the degree of polymerization, and also on the degree of saponification, which indicates the number of hydroxy groups. In solution, the number of inter- and intramolecular hydrogen bonds due to these differences affects the properties [37-44]. The physical properties of the solution at different concentrations and surface energy measurements showed differences in the viscosity gradient depending on the molecular weight and polymer concentration (**Supporting Information, Fig. S2**). The changes in viscosity due to differences in molecular weight can be explained using the Mark–Houwink–Sakurada equation $[\eta] = KM_w^{\alpha}$ for the relationship between intrinsic viscosity $[\eta]$ and molecular weight M_w [45,46]. The intrinsic viscosity was calculated to be 40 and 122 mL/g for an average molecular weight of 18 and 166 kg/mol, respectively ($\alpha = 0.50, K = 300 \times 10^{-3}$ mL/g [47]). This theoretical value is consistent with the intrinsic viscosity calculated from the viscosity measured by EMS (30 and 123 mL/g for molecular weights of 18 and 166 kg/mol, respectively) using Martin's equation $\ln \eta_{sp}/C = \ln[\eta] + K_M[\eta]C$, where η_{sp} is the specific viscosity, C is the weight-based concentration, and K_M is the Martin parameter [48].

Viscosity increased in an exponential-like manner with concentration, as observed in the semi-logarithmic plot (see Fig. S2A). The rate of this increase varied depending on the molecular weight. This trend is also supported by theoretical predictions based on Martin's equation, which accounts for the intrinsic chain properties and interchain interactions by incorporating both linear and exponential components (**Supporting Information, Fig. S3A**). From the viscosity–concentration master curve [49-53], two critical points, C^* and C^{**}, were obtained at which the slope changed (**Supporting Information, Fig. S3B**). As the molecular weight increases and the molecular chain becomes longer, the critical concentration C^* decreases, and the viscosity changes more drastically as the concentration changes. The critical concentration C^{**} at which the entanglement started was confirmed only for 166k PVA, suggesting that 18k PVA maintains a semi-dilute region, even at high concentrations. Therefore, the nucleation to form a vertical membrane requires a specific viscosity region.

Vertical membrane formation occurred when the viscosity was appropriate, humidity was high, and the interface remained fluid (see Fig. 2C). Based on this consideration, different drying conditions were tested using cells with pre-attached lids to maintain the internal humidity. We designed a cell with a lid on part of its aperture. Using this method, the evaporation rate was controlled, and the humidity at the evaporation interface was maintained, resulting in a long vertical membrane. By tuning the size of the aperture of the cell, horizontal polymer deposition was suppressed, and a vertical membrane was formed just below the aperture, showing meniscus splitting (**Fig. 3A**). The trend was also observed for PVA with a high saponification degree (**Supporting Information, Fig. S4**). During drying, the decrease in the liquid area depended on the size of the aperture (**Fig. 3B**). This suggested that the smaller the aperture, the more the humidity was maintained at the evaporation interface, which suppressed the drastic increase in viscosity at the interface. Humidity

retention is not affected by external humidity and is due to effective aperture design (**Supporting Information, Fig. S5**). The displacement velocity at the interface was measured using the same method as in previous studies [35], which depends on the shape of the nucleus (**Fig. 3C**). For an aperture of 3 mm, the descending speed of the interface exhibited monotonicity. In contrast, larger apertures, such as those of 5 or 10 mm, showed plateau states, indicative of the horizontal deformation of the interface. When the interface does not descend monotonically and a plateau region appears, a "Γ-shaped membrane" with an oblong circle of nuclei is formed. When the aperture size was further reduced, the nucleus changed to a point shape. The minimum aperture size for nucleation was approximately 0.8 mm, and vertical membrane formation was not observed when the aperture size was smaller than this (**Supporting Information, Fig. S6**). The pre-attached lid above the cell prevented solidification from the contact line with the sidewall by maintaining the humidity. However, if the aperture is too large, solidification occurs at the center of the cell in contact with the outside dry air, resulting in an oblong circular nucleus.

In the case of a single aperture, one vertical membrane was formed with the nucleus length corresponding to the size of the aperture. To investigate how membrane formation changed, the number of apertures was increased. Using a cell with two apertures, membrane formation was compared when the apertures were separated from and in contact with the sidewalls (**Supporting Information, Movie S2**). Vertical membranes were formed after the horizontal interfacial displacement when the apertures and sidewalls were in contact (**Fig. 4A, left**). In contrast, when the apertures were separated from the sidewalls, vertical membranes formed directly below the apertures (**Fig. 4A, right**). These different interface behaviors during the initial drying process can be explained by humidity changes around the corners of the cells. The formation of the horizontal film and its starting point N_0 is suggested to be due to the air–liquid–solid three-phase contact line being exposed to air and fixed

during drying by the solidification of PVA (**Fig. 4B, left**). The three-phase contact line is the site where accumulation by capillary force is the strongly affects, and the contact line is pinned immediately. During drying, the three-phase contact lines are fixed because of the constant evaporation caused by the rapid decrease in relative humidity. As shown in **Fig. 4B, right**, N_0 formation is suppressed, and the starting point of vertical membrane formation, N_1, occurs from the initial drying stage. This is because the three-phase contact lines were not exposed, and the relative humidity was maintained at a high value.

The *Z* position and velocity of the descent of the interface are shown in **Fig. 4C** and **D**, respectively. When the apertures are separated from the sidewalls, the position of the interface decreased continuously and monotonically. In contrast, when the apertures are in contact with the sidewalls, two plateau periods are observed, which were caused by the horizontal deformation of the interface. The plateau period exhibited a negative velocity value, indicating that the interface in the central region increased slightly and was attracted by the horizontal deformation of the interface near the sidewall. This clearly suggested that the interface in the central region is still fluid, and no film has formed yet. A comparison of the two plateau periods revealed a large deceleration in the second plateau region involved in the formation of the right horizontal membrane, which was caused by polymer deposition and film formation in the horizontal direction. As the number of apertures was further increased, the interfacial deformation and membrane formation became more complex, and vertical membranes did not form according to the number of apertures (**Supporting Information, Fig. S7**). This was due to the proximity of the apertures, which reduced the individual functions of the apertures. These observations emphasize the complexity of membrane formation, which is influenced by the aperture width and position and affects the local humidity. Thus, the control of polymer deposition by the exterior environment allows for vertical membrane formation and meniscus splitting.

Conclusion

The deformation of the evaporative interface in the meniscus splitting phenomenon was investigated toward the universal design for the dry/wet non-equilibrium conditions in an open system. Controlled vertical membrane formation through meniscus splitting was successfully demonstrated with aqueous PVA systems using a cell aperture design. The geometric design of the aperture, including its size and position, directly affects the humidity gradient and interface deformation. In an open system with apertures, an initial meniscus with downward convexity was capable of transitioning into a meniscus with multiple upward convexities. This deformation was necessary for the splitting phenomena. The demonstration with PVA elucidated two types of transitions: downward-to-downward and downward-to-upward. Owing to the easy drying properties of PVA, controlling the initial viscosity and local humidity are important factors.Moreover, the aperture design allows the number of membranes to grow in the vertical direction. Thus, extending the study to a wider range of materials might reveal that meniscus splitting is independent of the chemical species, indicating that the underlying mechanism is governed by physical interactions. The successful validation of this behavior in a challenging system such as PVA provides a foundation for verifying its universality across a wide range of systems. This capacity for humidity-mediated control of interfacial deformation has profound implications not only for phenomenology but also for the creation of self-organizing materials [54–56]. We believe that its applicability extends to smart materials having oriented structures with controlled directional responses to various stimuli such as vapor [26], cations [34], and pH [36].

Data availability

The authors declare that all the data supporting the findings of this study are available in the Article and Supplementary Information files.

Acknowledgments

This study was supported by a Grant-in-Aid for SPRING (JPMJSP2102), Fusion-Oriented Research for Disruptive Science and Technology (JPMJFR201G) from the Japan Science and Technology Agency, Grant-in-Aid for Scientific Research B (JP23K21136) from the Japan Society for the Promotion of Science, and Continuation Grants for Young Researchers from the Asahi Glass Foundation.

Author Contributions

R.H. and K.O. wrote the manuscript. R.H conducted the experiments. All authors contributed to the interpretation of the results. K.O. supervised the study. All the authors reviewed the manuscript.

Competing interests

The authors declare no competing interests.

Correspondence and requests for materials should be addressed to Kosuke Okeyoshi.

Supporting Information

The Supplementary Information is available on the website.

Methods and experimental details (PDF)

Supporting movies

Deformation process for each initial concentration and molecular weight (Movie S1)

Interfacial behavior when the aperture is in contact with and separated from the sidewall (Movie S2)

Reference

(1) Prigogine I, Lefever R, Goldbeter A, et al. Symmetry breaking instabilities in biological systems. Nature. 1969;223:913–916.

(2) Al-Housseiny T, Tsai P, Stone HA. Control of interfacial instabilities using flow geometry. Nat Phys. 2012;8:747–750.

(3) Bunton P, Marin D, Stewart S, Meiburg E, De Wit A. Schlieren imaging of viscous fingering in a horizontal Hele-Shaw cell. Exp Fluids. 2016;57:28.

(4) Rakshe M, Gandhi P. Controlled viscous fingering in volatile fluid towards spontaneous evolution of ordered 3D patterns. Sci Rep. 2023;13:10610.

(5) Saffman PG, Taylor GI. The penetration of a fluid into a medium or Hele-Shaw cell containing a more viscous liquid. Proc R Soc Lond A. 1958;245:312-329.

(6) de Gennes PG, Wyart FB, Quere D. Capillary and wetting phenomena: Drops, bubbles, pearls, wave. Springer; 2004.

(7) Zhou J, Man X, Jiang Y, Doi M. Structure formation in soft-matter solutions induced by solvent evaporation. Adv Mater. 2017;29:1703769.

(8) Zang D, Tarafdar S, Tarasevich Y, Choudhury M, Dutta T. Evaporation of a droplet: From physics to applications. Phys Rep. 2019;804:1-56.

(9) Deegan RD, Bakajin O, Dupont TF, Huber G, Nagel SR, Witten TA. Capillary flow as the cause of ring stains from dried liquid drops. Nature. 1997;389:827-829.

(10) Cai Y, Newby Z. Marangoni flow-induced self-assembly of hexagonal and stripelike nanoparticle patterns. J Am Chem Soc. 2008;130:6076–6077.

(11) Marin AG, Gelderblom H, Lohse D, Snoeijer JH. Order-to-disorder transition in ring-shaped colloidal stains. Phys Rev Lett. 2011;107:085502.

(12) Takizawa M, Sazuka Y, Horigome K, et al. Self-organization of soft hydrogel microspheres during the evaporation of aqueous droplets. Langmuir. 2018;34:4515-4525.

(13) Babu D, Scanes R, Plamont R, et al. Acceleration of lipid reproduction by emergence of microscopic motion. Nat Commun. 2021;12:2959.

(14) Rey M, Walter J, Harrer J, et al. Versatile strategy for homogeneous drying patterns of dispersed particles. Nat Commun. 2022;13:2840.

(15) Smalyukh I, Zribi O, Butler J, Lavrentovich O, Wong G. Structure and dynamics of liquid crystalline pattern formation in drying droplets of DNA. Phys Rev Lett. 2006;96:177801.

(16) Nassar M, Gromer A, Favier D, et al. Horizontal drying fronts in films of colloidal dispersions: Influence of hydrostatic pressure and collective diffusion. Soft Matter. 2017;13:9162-9173.

(17) Chu G, Vilensky R, Vasilyev G, et al. Structure evolution and drying dynamics in sliding cholesteric cellulose nanocrystals. J Phys Chem Lett. 2018;9(8):1845-1851.

(18) Nuzzo M, Sloth J, Bergenstahl B, Millqvist-Fureby A. Phase segregation in individually dried particles composed of biopolymers. Langmuir. 2015;31(40):10946-10954.

(19) Almohammadi H, Fu Y, Mezzenga R. Evaporation-driven liquid–liquid crystalline phase separation in droplets of anisotropic colloids. ACS Nano. 2023;17(3):3098-3106.

(20) Tanaka T, Sun ST, Hirokawa Y, et al. Mechanical instability of gels at the phase transition. Nature. 1987;325:796-798.

(21) Yoshida R, Uchida K, Kaneko Y, et al. Comb-type grafted hydrogels with rapid de-swelling response to temperature change. Nature. 1995;374:240–242.

(22) Meloy-Gorr H, Zueger J, Barnard J. Lysozyme pattern formation in evaporating drops. Langmuir. 2012;28(9):4039-4042.

(23) Kim J, Cho K, Ryu S, Kim S, Weon B. Crack formation and prevention in colloidal drops. Sci Rep. 2015;5:13166.

(24) Okeyoshi K, Okajima MK, Kaneko T. Emergence of polysaccharide membrane walls through macrospace partitioning via interfacial instability. Sci Rep. 2017;7:5615.

(25) Okeyoshi K, Joshi G, Okajima MK, Kaneko T. Formation of polysaccharide membranes by splitting of evaporative air–LC interface. Adv Mater Interfaces. 2018;1701:219.

(26) Budpud K, Okeyoshi K, Okajima MK, Kaneko T. Vapor-sensitive materials from polysaccharide fibers with self-assembling twisted microstructures. Small. 2020;16:2001993.

(27) Okeyoshi K. DRY & WET: Meniscus splitting from a mixture of polysaccharides and water. Polymer J. 2020;52:1185.

(28) Samid-Merzel N, Lipson S. G, Tannhauser D. S. Pattern formation in drying water films. Phys. Rev. E. 1998;57:2906-2913.

(29) Okubo T, Tsuchida A, Kokufuta E. Drying dissipative structures of gelatin solution. Colloid Polym Sci. 2015;293:1583-1591.

(30) Parasa M, Harmand S, Sefiane K. Mechanisms of pattern formation from dried sessile drops. Adv Colloid Interface Sci. 2018;254:22-47.

(31) Joshi G, Okeyoshi K, Mitsumata T, Kaneko T. Micro-deposition control of polysaccharides on evaporative air-LC interface to design quickly swelling hydrogels. J Colloid Inter Sci. 2019;546:184-191.

(32) Okeyoshi K, Yamashita M, Budpud K, Joshi G, Kaneko T. Convective meniscus splitting of polysaccharide microparticles on various surfaces. Sci Rep. 2021;11:767.

(33) Joshi G, Okeyoshi K, Yusof F, et al. Interfacial self-assembly of polysaccharide rods and platelets bridging over capillary lengths. J Colloid Interface Sci. 2021;591:483-489.

(34) Saito I, Wu L, Hara M, et al. Anisotropic responses with cation selectivity in hierarchically ordered polysaccharide networks. ACS Appl Polym Mater. 2022;4:7054−7060.

(35) Wu L, Saito I, Hongo K, Okeyoshi K. Recognition of spatial finiteness in meniscus splitting based on evaporative interface fluctuations. Adv Mater Interfaces. 2023;10:2300510.

(36) Nguyen T, Tonomura Y, Ito N, et al. Reconstruction of chitosan network orders using the meniscus splitting method for designing pH-responsive materials. Langmuir. 2024;40:11927-1193.

(37) Buslov DK, Sushko NI, Tretinnikov ON. IR investigation of hydrogen bonds in weakly hydrated films of poly(vinyl alcohol). Polym Sci Ser A. 2011;53:1121–1127.

(38) Baker MI, Walsh SP, Schwartz Z, et al. A review of polyvinyl alcohol and its uses in cartilage and orthopedic applications. J Biomed Mater Res B Appl Biomater. 2012;100B:1451–1457.

(39) Song P, Xu Z, Guo Q. Bioinspired strategy to reinforce PVA with improved toughness and thermal properties via hydrogen-bond self-assembly. ACS Macro Lett. 2013;2(12):1100–1104.

(40) Wolf S, Hartl B, Carroll C, Neel MC, Greenwald DN. Beyond PVA: why recovery under the Endangered Species Act is more than population viability. BioScience. 2015;65(2):200–207.

(41) Kumar A, Han SS. PVA-based hydrogels for tissue engineering: a review. Int J Polym Mater. 2016;66(4):159–182.

(42) Abdullah ZW, Dong Y, Davies IJ, et al. PVA, PVA blends, and their nanocomposites for biodegradable packaging application. Polym Plast Technol. 2017;56(12):1307–1344.

(43) Sapalidis AA. Porous polyvinyl alcohol membranes: preparation methods and applications. Symmetry. 2020;12(6):960.

(44) Fu Z, Guo S, Li C, et al. Hydrogen-bond-dominated mechanical stretchability in PVA films: from phenomenological to numerical insights. Phys Chem Chem Phys. 2022;24:1885–1895.

(45) Flory PJ. Principles of polymer chemistry. Ithaca, NY: Cornell University Press; 1953. p. 266–316.

(46) Tanford C. Physical chemistry of macromolecules. New York: John Wiley Press; 1961. p. 390–412.

(47) Mohsen-Nia M, Modarress H. Viscometric study of aqueous poly(vinyl alcohol) (PVA) solutions as a binder in adhesive formulations. J Adhes Sci Technol. 2006;20(12):1273–1280.

(48) Martin AF. Toward a referee viscosity method for cellulose. Tappi. 1951;34(8):363–366.

(49) Hong PD, Chou CM, He CH. Solvent effects on aggregation behavior of polyvinyl alcohol solutions. Polymer. 2001;42:6105–6112.

(50) Krause WE, Bellomo EG, Colby RH. Rheology of sodium hyaluronate under physiological conditions. Biomacromolecules. 2001;2:65–69.

(51) Muller F, Jean B, Perrin P, et al. Mechanism of associations of neutral semiflexible biopolymers in water: the xyloglucan case reveals inherent links. Macromol Chem Phys. 2013;214:2312–2323.

(52) Elmarhoum S, Ako K. Lower critical concentration temperature as thermodynamic origin of syneresis: case of kappa-carrageenan solution. Carbohydr Polym. 2021;267:118191.

(53) Kol R, Nachtergaele P, De Somer T, et al. Toward more universal prediction of polymer solution viscosity for solvent-based recycling. Ind Eng Chem Res. 2022;61:10999−11011.

(54) Yoshida R. Self-oscillating gels driven by the Belousov-Zhabotinsky reaction as novel smart materials. Adv Mater. 2010;22:3463–3483.

(55) Nguindjel AC, de Visser PJ, Winkens M, Korevaar PA. Spatial programming of self-organizing chemical systems using sustained physicochemical gradients from reaction, diffusion, and hydrodynamics. Phys Chem Chem Phys. 2022;24:23980.

(56) Kawamata K, Nishiyama K, Matsumoto D, et al. Autonomous assembly and disassembly of gliding molecular robots regulated by a DNA-based molecular controller. Sci Adv. 2024;10:eadn4490.

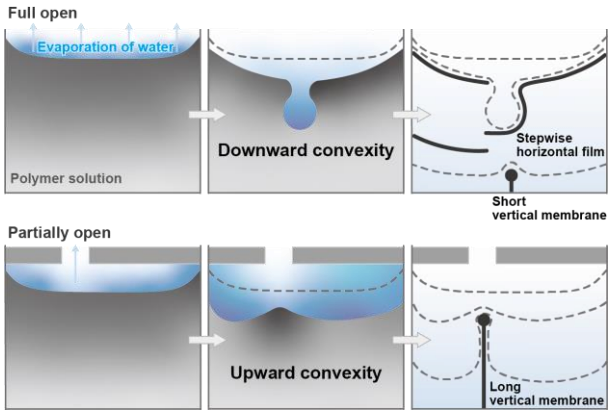

Fig. 1 The strategic design of aperture configurations enables the regulation of interfacial convexity through localized humidity modulation. In a fully open cell, accelerated solvent evaporation from the polymer solution induces downward interfacial deformation followed by vertical membrane growth. In contrast, a partially open cell maintains elevated local moisture levels to suppress solvent evaporation and promote vertical membrane formation from the start due to upward interface deformation.

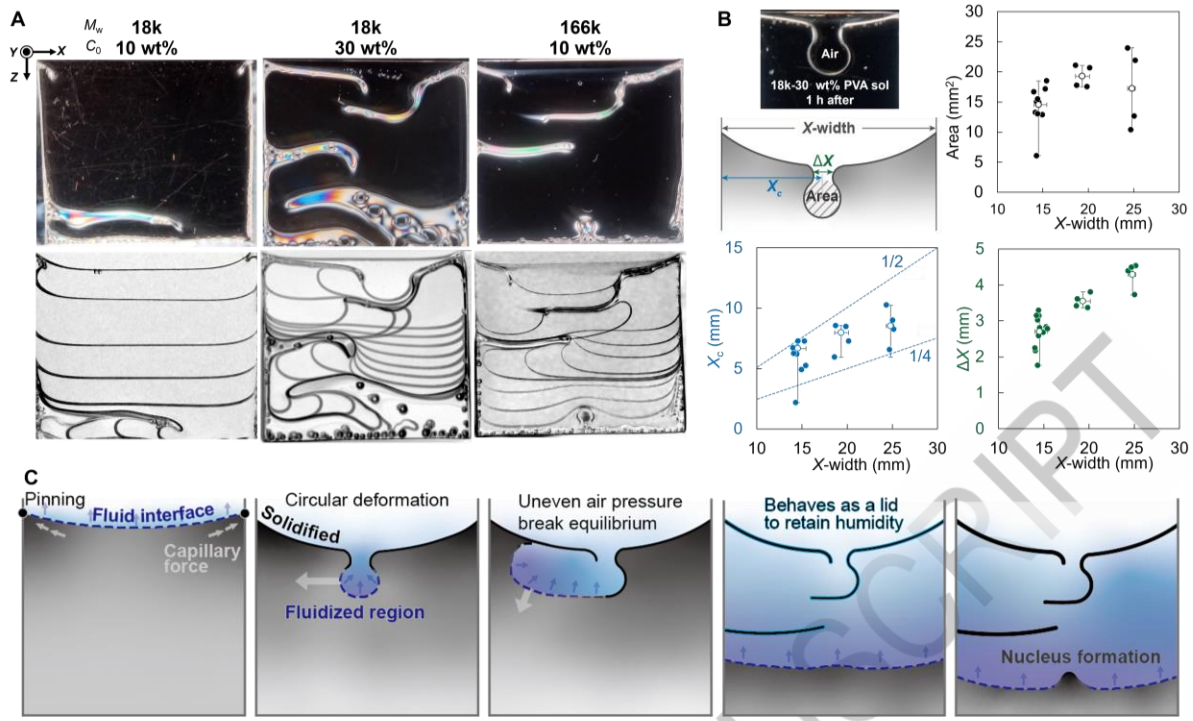

Fig. 2 Interfacial shape changes into downward convex and polymer deposition in the horizontal direction in a fully open aperture cell. A. Images of drying interface (upper) and superimposition of the time evolution (lower) of PVA solutions with different molecular weights (M_w) and initial concentrations (C_0). The number of images for superpositions: 10 during 30 h (18k, 10 wt%), 20 during 65 h (18k, 30 wt%), 15 during 60 h (166k, 10wt%); cell size: 25 mm-width, 1 mm-gap, ~20 mm-depth; drying temperature: 60 °C; relative humidity outside of the cell: ~5%. **B.** Geometric analysis of the air hole during the down-convex interfacial change of the 18k-30 wt% PVA solution in different cells, *X*-width, 1 mm-gap, ~20 mm-depth, where *X* = ~15, ~20, and ~25 mm. **C.** Schematic of the interface shape transition in the 166k-10 wt% PVA solution.

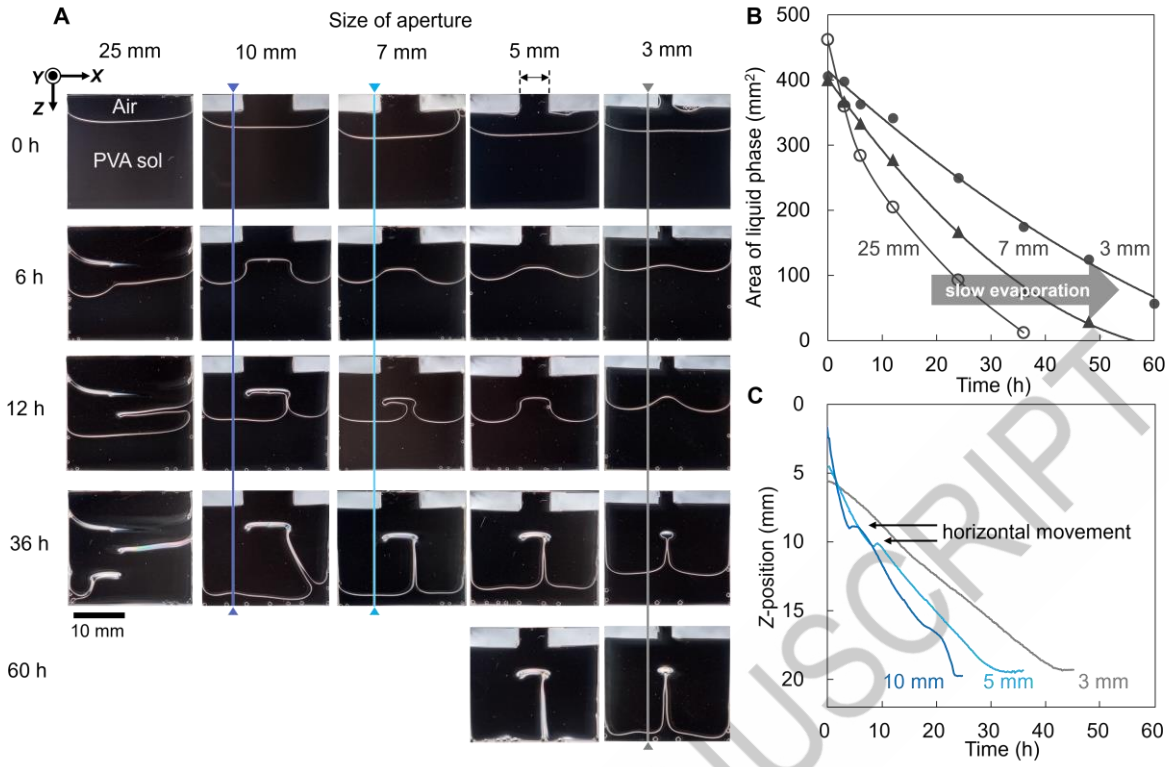

Fig. 3 Open system for water evaporation and specific polymer deposition. A. Time course images of polymer deposition from cells with various aperture sizes. **B.** Decrease in the liquid area in the XZ plane for different given aperture sizes. **C.** Displacement velocity of the interface at the positions depicted in A. Initial solution concentration: 10 wt% PVA (M_w ~166k); cell size: 25 mm-width, 1 mm-gap, ~20 mm-depth; drying temperature: 60 °C; relative humidity outside of cells: ~5%.

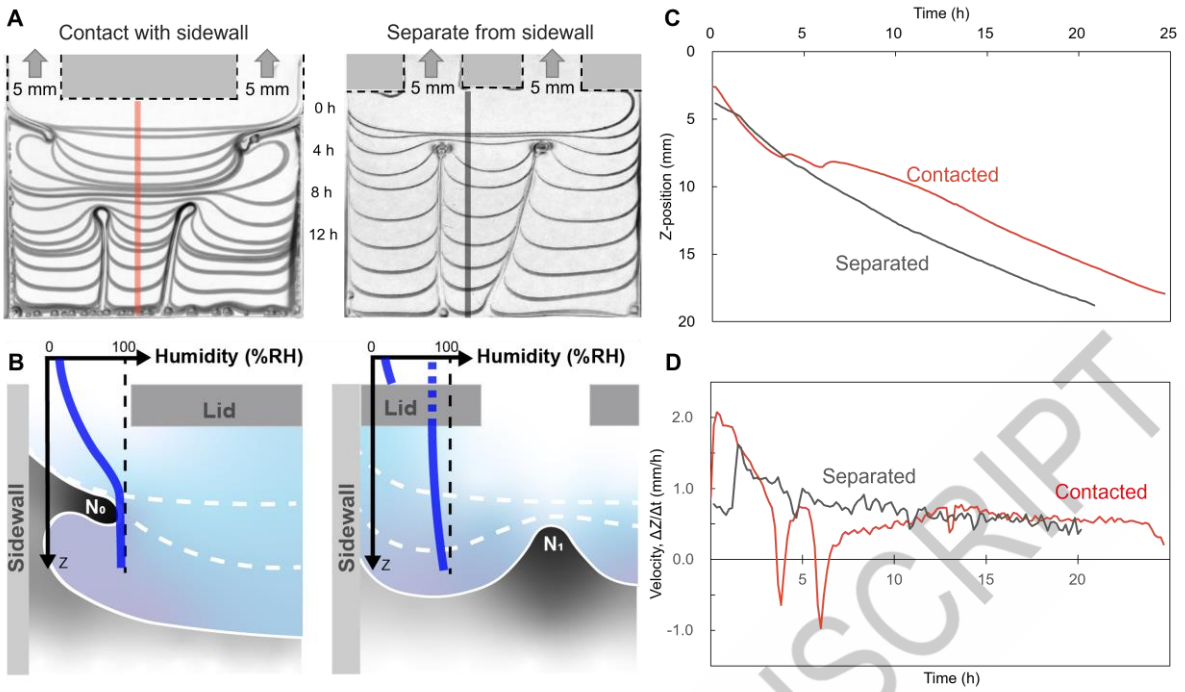

Fig. 4 Role of the airflow pathway in the air phase. A. Superimposition of the time evolution of interface shapes for two apertures in contact with (left) and separated from the sidewalls (right). **B.** Schematic of humidity distribution in the area 5 mm from the sidewall with the airflow pathway along/not along the sidewall. **C.** Time course of the interface in the Z direction at the position depicted in A, close to the center of the cell. **D.** Time course of evaporation velocity for each aperture shape. Initial solution concentration: 10 wt% PVA (M_w ~166k); cell size: 25 mm-width, 1 mm-gap, ~20 mm-depth; drying temperature: 60 °C; relative humidity outside of cells: ~5%.

Supplementary Information

Design of open systems for meniscus splitting using an aqueous polymer solution

Reina Hagiwara[1], Kosuke Okeyoshi[1*]

[1]Graduate School of Advanced Science and Technology, Japan Advanced Institute of Science and Technology, 1-1 Asahidai, Nomi, Ishikawa 923-1292, Japan

* Correspondence should be addressed.
E-mail: okeyoshi@jaist.ac.jp

Table of Contents

I. Experimental methods

Materials

Polyvinyl alcohol with molecular weights (M_w) of 13—23 (PVA-18k) and 146—186 kg/mol (PVA-166k) (87–89% hydrolyzed) were purchased from Sigma-Aldrich. The aqueous PVA solution was prepared by dispersing the polymer powder in pure water, stirring at room temperature (~ 25 °C) for 1 h, heating it in a 90 °C water bath for 2 h, then stirring at room temperature for 1 h. The solution samples were stored at room temperature.

Drying experiment

Drying experiments were performed by injecting the polymer solution into a top-open cell with a narrow gap, as shown in **Fig. S1A**. The Hele–Shaw cell consisted of two glass slides (S1111, Matsunami Glass Ind. Ltd.) and a polyvinyl chloride (PVC) sheet that is inert under thermal conditions during drying, and easy to prepare the customized size cells. Whereas a small amount of bubbles are generated from the spacer during the long heating, the amount is much smaller than in other materials such as silicone rubber. The open system was designed by changing the shape of the PVC sheet. The samples were placed in an oven (VOS-210C, EYELA) with an air circulator maintained at constant temperature under atmospheric pressure. In the drying experiments for the spatiotemporal analysis, the samples were placed in an observation box (**Fig. S1B**). The temperature and humidity of the observation box were controlled using a heat pen connected to a circulation tube and a rubber heater on the inner wall of the box. Dry air from the pen heater flowed into the observation box as shown in **Fig. S1C**, keeping the temperature and humidity constant (**Fig. S1D**). Interface changes during drying were monitored using two orthogonally assembled polarizers and a first-order retardation plate (λ = 530 nm), and images were taken at 10-minute intervals.

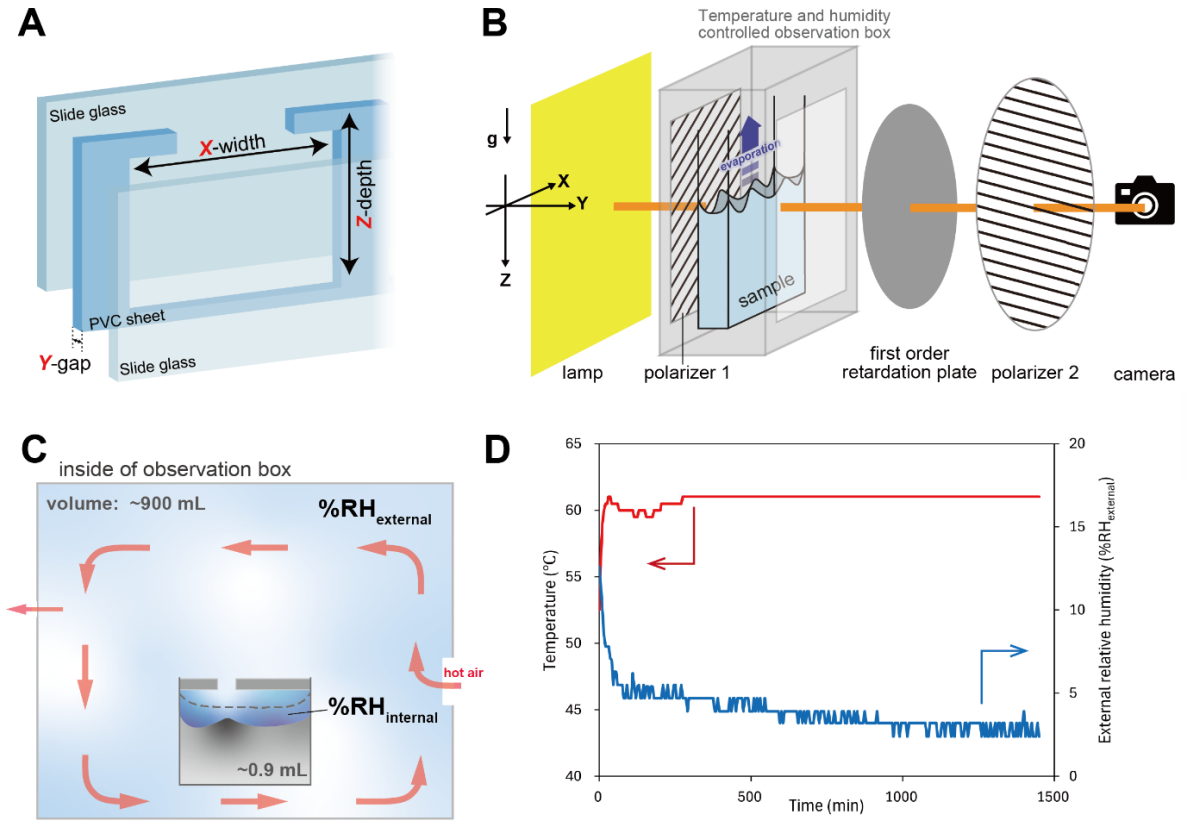

Fig. S1 Schematic of the experimental setup. **A.** Cell details. The size of the cell is indicated by the *X*-width, *Y*-gap, and *Z*-depth. **B.** Observation box installation conditions and environment. **C.** Dry air flow in the observation box. **D.** Time variation of temperature and humidity in the observation box.

II. Characterization of the PVA solution

The viscosity (η) and density (ρ) of the solutions were measured over a wide concentration range for each molecular weight PVA solution (**Fig. S2A** and **B**). The viscosity was measured using a non-contact electromagnetic spinning method using an EMS-1000S (Kyoto Electronics Manufacturing Co., Ltd.), and the density was measured using an oscillatory method based on the U-tube oscillation principle with a DMA 4501 (Anton Paar). The contact angle (θ) and surface tension (γ) were measured using a DMs-401 instrument (Kyowa Interface Science Co., Ltd.) (**Fig. S2C**). The capillary length l was calculated using Equation 1, where g is the acceleration owing to gravity (9.8 m/s^2).

$$l = \sqrt{\gamma/\rho g} \quad (1)$$

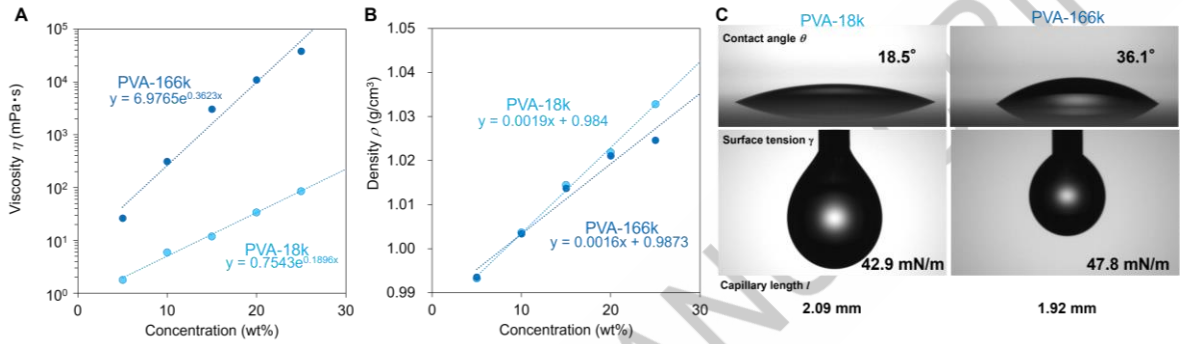

Fig. S2 Physical properties of PVA at different molecular weights. **A.** Viscosity of each aqueous polymer solution. **B.** Density of each aqueous polymer solution. **C.** Difference in surface energy. Contact angle on glass (upper), surface tension (middle), and capillary length (bottom).

Among the five datasets, the viscosity and contact angle showed remarkable differences depending on the molecular weight of PVA. Although the contact angle changed twice, the effect was considered to be small because both angles were low. Major changes appeared in both the intrinsic viscosity and the rate of increase in viscosity. **Fig. S3A** shows a graph of $\ln \eta_{sp}/C$ as a function of concentration. The intrinsic viscosity is calculated from the slope of this graph based on Martin's equation (Equation 2). Specific viscosity η_{sp} is given by $(\eta/\eta_0) - 1$, where η is the measured value and η_0 is the viscosity of water (0.47 mPa·s). The calculated intrinsic viscosity was similar to the theoretical value (40 and 122 mL/g of 18 and 166 kg/mol, respectively) based on the Mark–Houwink–Sakurada equation: $[\eta] = KM_w^{\alpha}$. Next, using a log–log plot of η_{sp} versus the dimensionless coil overlap parameter $C[\eta]$ for the slope of the viscosity increase (**Fig. S3B**), three regions corresponding to the dilute, semidilute, and concentrated domains were identifiable. Within each domain, the η_{sp}–$C[\eta]$ relationship is described by a linear dependence, with transitions from one domain to another accompanied by a change in the slope, as indicated by the critical concentrations C^* and C^{**}. For PVA-18k, the slopes are 1.2 and 2.5, and the critical concentration C^* resulting from the

initial point of contact between individual chains was 4.7 wt%. In contrast, for PVA-166k, the slopes were 1.5, 3.3, and 4.8, with a C^* of 2.5 wt% and a C^{**} of 6.3 wt% as the initial point of the entanglement of the polymer chains.

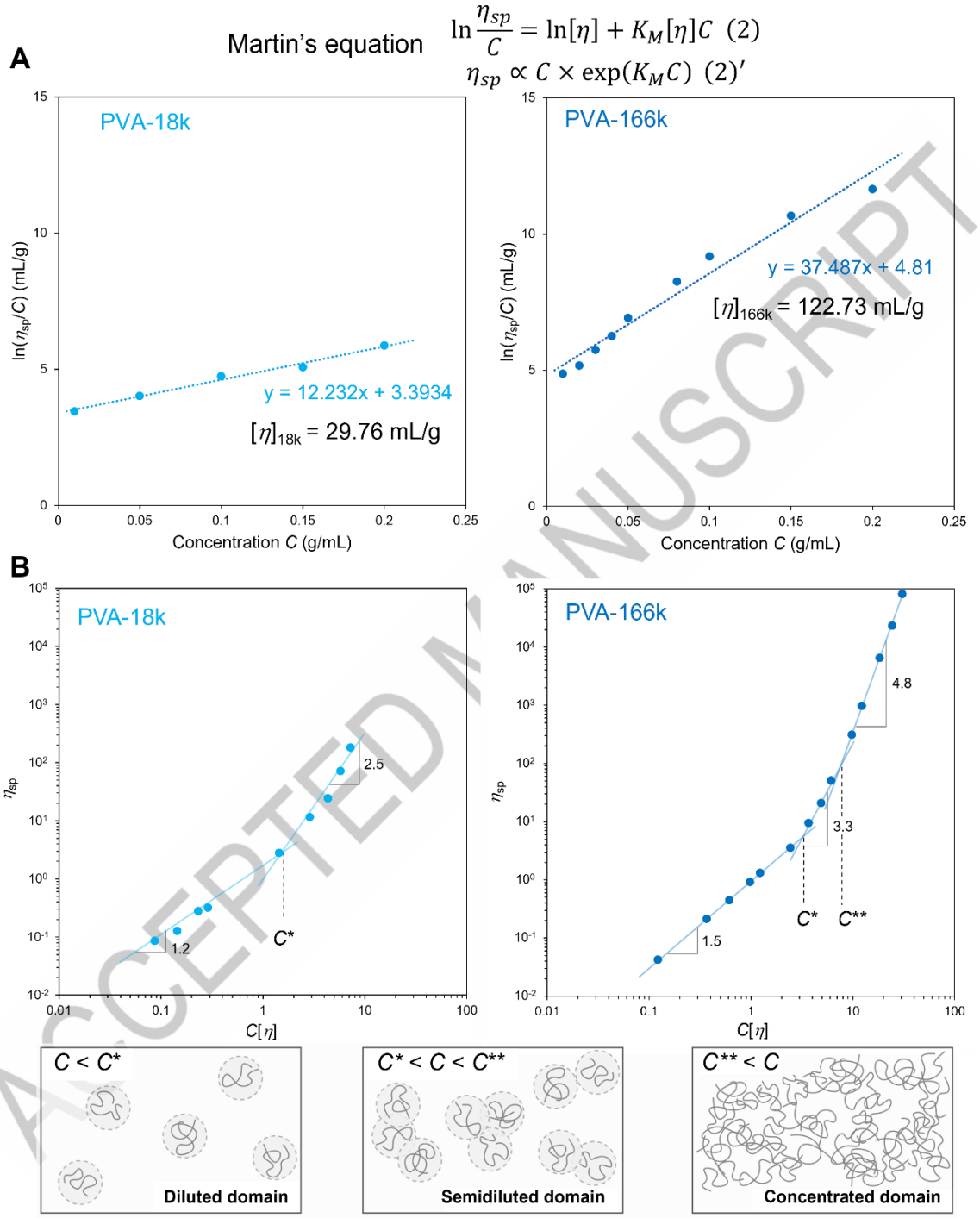

Fig. S3 The equation for viscosity gradient as a function of polymer concentration. **A.** Calculation of intrinsic viscosity using Martin's equation. **B.** Log–log plots of η_{sp} versus $C[\eta]$ of PVA with a molecular weight of 13—23 (left) and 146—186 (right)kg/mol and the corresponding models of chain aggregation for each.

III. Membrane shape formed by aperture design

The drying results for higher saponification degree (~100%) PVA solutions are shown in **Fig. S4**. The PVA with a higher saponification degree results in lower solubility, and the aqueous solution shows higher viscosity. The main materials used in this study had a saponification degree of 88% and a molecular weight of 166k. A comparison was made using initial viscosity about half or twice as high as it, and almost the same membrane formation was observed just below the initial interface. The similarity in membrane shape indicates that these samples are concentrated regions with entanglement above *C***, and there is no noticeable difference in dehydration characteristics by saponification degree.

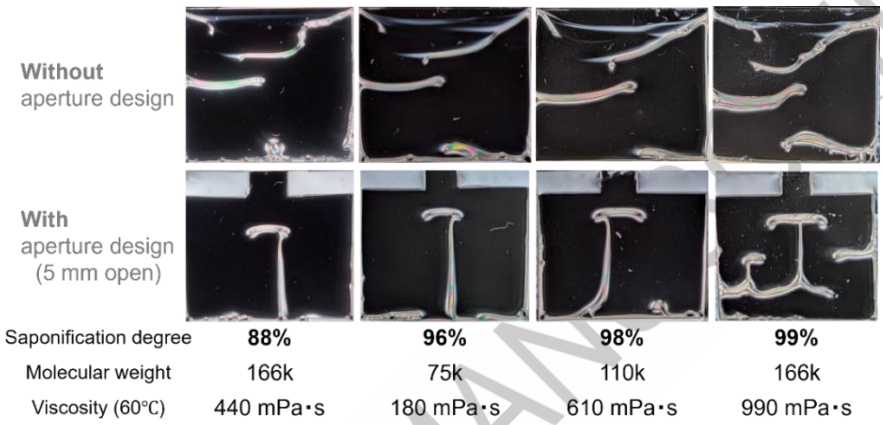

Fig. S4 Membrane shape for each saponification degree. Initial solution concentration: 10 wt% PVA; cell size: 25 mm-width, 1 mm-gap, ~20 mm-depth; drying temperature: 60 °C; relative humidity outside of cells: ~5%.

At lower drying temperatures and higher external humidity (40℃, ~10%RH), similarly shaped membranes were formed in the aperture-design cells (**Fig. S5**). This indicates that the internal humidity near the evaporation interface is more important than the external humidity.

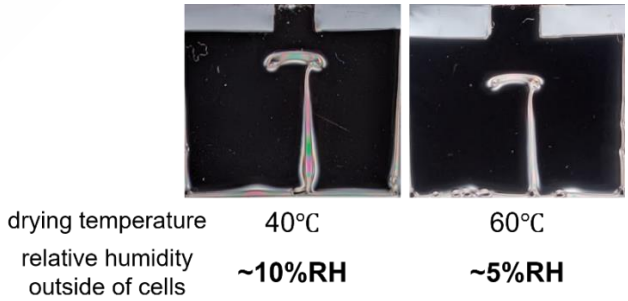

Fig. S5 Membrane formation under different conditions outside the cell. Initial solution concentration: 10 wt% PVA; cell size: 25 mm-width, 1 mm-gap, ~20 mm-depth, aperture size ~5 mm.

When the aperture size was reduced from the full aperture size (25 mm), similar vertical membrane formation was observed in the aperture size range of 1–10 mm. As shown in **Fig. S6**, a vertical membrane was not observed when the aperture size was smaller than 0.8 mm. This is because the interfacial fluctuations cannot grow nonlinearly with the observed time at this drying temperature and humidity condition of the evaporation interface. Therefore, it is possible to induce nucleation by changing the depth of the cell to increase the observation time

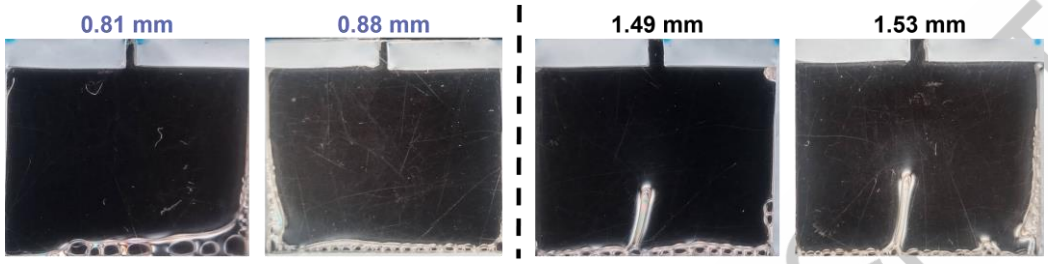

Fig. S6 Minimum aperture length for nucleation. Initial solution concentration: 10 wt% PVA (M_w ~166k); cell size: 25 mm-width, 1 mm-gap, ~20 mm-depth; drying temperature: 60 °C; relative humidity outside of cells: ~5%.

Fig. S7 shows the results of the drying experiments in a cell with three apertures. Vertical membranes were not formed according to the number of apertures, either when the apertures at both ends were in contact with or separated from the sidewalls. It is possible that the individual functions of the apertures were reduced because of their proximity to each other. When the aperture was in contact with the sidewall, a starting point of horizontal film N_0 formed initially, as in the cell with two apertures; however, the stepwise horizontal film formation continued. Even when the apertures were far from the sidewalls, a N_0 was formed because the distance between the apertures and sidewalls was so small that humidity control near the sidewalls was ineffective.

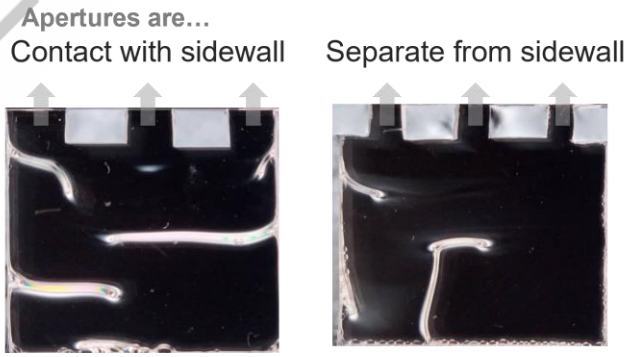

Fig. S7 The complex membrane formation in a cell with three apertures. Initial solution concentration: 10 wt% PVA (M_w ~166k); cell size: 25 mm-width, 1 mm-gap, ~20 mm-depth; drying temperature: 60 °C; relative humidity outside of cells: ~5%.

[[Graphical Abstract]]